

# Electrochemical Properties of Fused Pyrimidine-Triazole Heterocyclic Molecules as Novel Drug Candidates

## Short title: Electrochemical Properties of Pyrimidine-Triazole Heterocyclic Molecules

Fatma Kurul<sup>1</sup>, Hüseyin Istanbulu<sup>2</sup>, Hüseyin Oğuzhan Kaya<sup>3</sup>, Arif E. Cetin<sup>4</sup>, Seda Nur Topkaya<sup>3</sup>

<sup>1</sup>Izmir International Biomedicine and Genome Institute, Dokuz Eylul University

<sup>2</sup>Department of Pharmaceutical Chemistry, Faculty of Pharmacy, Izmir Katip Celebi University

<sup>3</sup>Department of Analytical Chemistry, Faculty of Pharmacy, Izmir Katip Celebi University

<sup>4</sup>Izmir Biomedicine and Genome Center, Balçova, Izmir 35340, Turkey

### Corresponding Author Information

Seda Nur Topkaya

sedanur6@gmail.com

14.02.2023

13.05.2023

16.05.2023

### ABSTRACT

**INTRODUCTION:** Triazolopyrimidinones are a type of compound used in medicinal chemistry. In this study, three novel triazolopyrimidinone derivatives were synthesized as drug candidates which are named ((5-(Chloromethyl)-2-(4-methoxyphenyl)-[1,2,4]triazolo[1,5-a]pyrimidin-7(3H)-one) (S1-TP), 2-(4-Methoxyphenyl)-5-(piperidinomethyl)-[1,2,4]triazolo[1,5-a]pyrimidin-7(3H)-one (S2-TP), and 2-(4-Methoxyphenyl)-5-(morpholinomethyl)-[1,2,4]triazolo[1,5-a]pyrimidin-7(3H)-one (S3-TP). Their electrochemical properties were investigated for the first time with voltammetric techniques on carbon graphite electrodes. Moreover, stability tests for each drug candidate were performed on different days. After revealing the electrochemical properties of drug candidates, their effect on double-stranded (ds) DNA was examined by measuring the oxidation currents of the guanine of dsDNA before and after the interaction.

**METHODS:** An electrochemical setup that included a pencil graphite electrode as the working electrode, an Ag/AgCl reference electrode, and a platinum wire as the auxiliary electrode was used in this study. The experiments for optimum pH, scan rate, and concentration of drug candidates were conducted. The interaction between Ss-TP and dsDNA was evaluated using differential pulse voltammetry. The stability of each drug candidate was tested on various days.

**RESULTS:** A comprehensive characterization of the S1-TP, S2-TP and S3-TP compounds was studied for the first time. This study showed that the electrochemical oxidation of S1-TP and S2-TP was irreversible and diffusion-controlled. Additionally, the transfer of electrons in S3-TP was controlled by adsorption. The interaction between Ss-TP and dsDNA resulted in notable changes in the dsDNA peak potential. The dsDNA peak potential shifted negatively after interaction with S1-TP, S2-TP, and S3-TP. Under optimum conditions, the detection limits for S1-TP, S2-TP, and S3-TP were 1.5 µg/mL, 1.0 µg/mL, and 2.0 µg/mL, respectively.

**DISCUSSION AND CONCLUSION:** From our experimental data, we concluded that these molecules can be used as drug molecules for their remarkable effects on DNA.

**Keywords:** Drug Candidate, Drug, DNA, Drug-DNA Interaction, Triazolopyrimidinone, Heterocyclic compounds.

## 1. INTRODUCTION

Triazolopyrimidinones, a class of fused pyrimidinone-triazole heterocyclic ring systems, are considered privileged scaffolds in medicinal chemistry. A wide range of bioactivity of the triazolopyrimidinone bearing compounds has been reported as FABPs, ferrochelatase, and PAS Kinase inhibitors (1,2). Additionally, triazolopyrimidinones and triazolopyrimidines with purine bioisosteric analogues are reported to have anticancer activity through various mechanisms (3). Fandzloch et al. reported that triazolopyrimidine ruthenium(II) complexes show anticancer activity on various cancer cell lines, and these complexes bind to the minor groove of DNA or intercalate it (4). In another study, triazolopyrimidine copper(II) complexes and their DNA intercalating capacity were analyzed with absorption and fluorescence spectrums (5). The results suggested that the complexes were intercalated into DNA strands as well as their damage through metallonuclease activity. Harrison et al. discovered a selective and highly soluble triazolopyrimidone derivative molecule as an NLRP3 inflammasome inhibitor using *in silico* pharmacophore model, which could be used as an inhibitor for the treatment of inflammatory diseases (6).

Drug and drug candidates can interact with DNA in several ways, and the interaction between them can be determined with various instrumental methods such as circular dichroism (CD), nuclear magnetic resonance (NMR), Fourier transform infrared spectroscopy (FTIR), viscosity measurements, infrared spectroscopy (IR), mass spectrometry (MS), molecular docking, and electrochemical methods (7–15). Morawska et al. developed a voltammetric method to observe the electrochemical behavior of tenofovir and its interaction mechanism with ds/ssDNA, and compared their method with spectrophotometric analyses, where the electrochemical method showed better analytical performance compared to spectrophotometry in terms of LOD and linear range (11). In another study, the interaction mechanism of mitoxantrone and DNA molecule was studied employing FTIR, UV–Vis, and CD. According to spectroscopic results, mitoxantrone possibly binds to DNA from guanine (N7), thymine (O2) and cytosine (O2) locations (16). Electrochemical methods are preferred due to their rapidness, high selectivity, low instrumentation cost, simple operation, and portability. They could reveal the chemical properties and potential toxic effects of drug candidates and determine the metabolic processes (17).

The main interaction modes between the drug molecules and DNA can be simply classified as covalent and non-covalent binding. Among them, covalent binding with DNA is irreversible, inhibits the functions of DNA, and leads to cell death. Contrarily, non-covalent binding is reversible, and they are sub-classified as electrostatic, groove, and intercalative bindings. Electrostatic binding results from the interactions of positively charged ligands with the negatively charged DNA phosphate backbone structure. Groove binding is also sub-categorized as minor and major groove binding which small ligands bind to the minor or major groove of DNA by van der Waals or and hydrogen bonds. Small ligands could bind to DNA via unique binding sites and this mode is called as intercalation. In this mode, Intercalators containing planar heterocycle groups could slide and stack between base pairs of DNA and stabilize the duplex without breaking the base pair or forming covalent bonds.

Our study is the first report analyzing the electrochemical properties of novel triazolopyrimidinone derivatives as purine analog chemical structures. First, we investigated the electrochemical properties of novel drug candidates, and then their interaction with dsDNA was analyzed with voltammetric methods as Differential Pulse Voltammetry (DPV) and Cyclic Voltammetry (CV). Experimental parameters, e.g., pH, concentration of drug candidates, and scan rate were examined for revealing the analytical properties of these novel drug candidates. Stability tests were performed with optimal storage conditions and within different days to observe the shelf life of the drug candidates.

## 2. MATERIALS AND METHODS

### 2.1 Materials

The salmon sperm DNA used in this experiment (Sigma Aldrich, purity  $\geq 98\%$ ) was dissolved in deionized water to prepare stock solutions. 3-amino-5-(methylthio)-4H-1,2,4-triazole (Merck, purity  $\geq 97\%$ ) and chloroform (Alfa Aesar-Acros Organics, purity  $\geq 99\%$ ) were used as received without further purification. The buffers were prepared using analytical grade chemicals from various from different companies as Carlo Erba, Alfa Thermo Fisher Scientific, and Isolab. In the experiments, we used 0.5 M Acetate (ACB, pH: 3.8, 4.8, 5.6) and 0.05 M Phosphate (PBS, pH: 7.4) buffers involving 0.02 M NaCl and 0.05 M Tris-EDTA (TE, pH: 8.0) buffer.

### 2.2 Instrumentation

Analytical thin layer chromatography (TLC) was used with Merck silica gel F-254 plates. Melting points were employed with Stuart SMP 30 (Staffordshire, ST15 OSA). NMR spectra were reported with Varian AS 400 Mercury plus NMR (Varian Inc.) spectrometer at 400 MHz for  $^1\text{H}$  and 100 MHz for  $^{13}\text{C}$  using DMSO-*d*<sub>6</sub> as solvent. The coupling constants (J) were presented in Hertz (Hz) without internal standard. Splitting patterns were designated as follows: s (singlet); d (doublet); t (triplet); p (pentet) and m (multiplet). HR-MS were determined on Agilent 6200 Series TOF and 6500 Series Q-TOF LC/MS System with ESI (+) ionization. Microwave irradiation (MW) synthesis of

the compounds was conducted on Milestone MicroSYNTH (Milestone S.r.l.) microwave apparatus. PalmSens4 handheld analyzer with PStTrace 5.8 software were used for electrochemical studies. Pencil graphite electrodes were employed as working electrodes. To complete the three-electrode system, a platinum wire and an Ag/AgCl electrode were employed as auxiliary and reference electrodes, respectively.

### 2.3 Experimental

#### 2.3.1 General Synthesis of Drug Candidates

The synthesis steps are shown in Figure 1.

##### *Synthesis of substituted triazole*

5-(4-methoxyphenyl)-3-amino-1,2,4-triazole was synthesized according to reference (18). In the first step, aminoguanidine bicarbonate and 4-methoxybenzoyl chloride were reacted. Later, the amide derivative underwent cyclization to yield 5-(4-methoxyphenyl)3-aminotriazole.

##### *Synthesis of S<sub>1</sub>-TP*

5-(4-methoxyphenyl)-3-amino-1,2,4-triazole (10 mmol) and ethyl 4-chloroacetoacetate (20 mmol) were mixed in 18 mL acetic acid (MW, 20 min, 180°C). The formed solid was filtered off, rinsed with acetic acid, and dried. These steps resulted to yield S<sub>1</sub>-TP (5-(Chloromethyl)-2-(4-methoxyphenyl)-[1,2,4]triazolo[1,5-*a*]pyrimidin-7(3*H*)-one, which was used in the next steps without purification.

##### *Synthesis of S<sub>2</sub>-TP and S<sub>3</sub>-TP*

In the last step of the synthesis, the nucleophilic substitution of the obtained S<sub>1</sub>-TP with piperidine and morpholine yield S<sub>2</sub>-TP and S<sub>3</sub>-TP. S<sub>1</sub>-TP (1 mmol) and amine derivatives namely, piperidine/morpholine (2 mmol) were stirred in 16 mL DMF in the presence of 1.5 mmol caesium carbonate (Cs<sub>2</sub>CO<sub>3</sub>) using MW irradiation (150 W, 15-30 min, 95°C). The excess of Cs<sub>2</sub>CO<sub>3</sub> was filtered, and the filtrate was concentrated under reduced pressure. This mixture was further purified by column chromatography over silica gel 60 (70-230 mesh ASTM, Merck) with chloroform:methanol (10:2) and the compounds were recrystallized from methanol or acetone. The crude yield is 40-45 %.

**S<sub>2</sub>-TP:** 2-(4-Methoxyphenyl)-5-(piperidinomethyl)-[1,2,4]triazolo[1,5-*a*]pyrimidin-7(3*H*)-one

**S<sub>3</sub>-TP:** 2-(4-Methoxyphenyl)-5-(morpholinomethyl)-[1,2,4]triazolo[1,5-*a*]pyrimidin-7(3*H*)-one

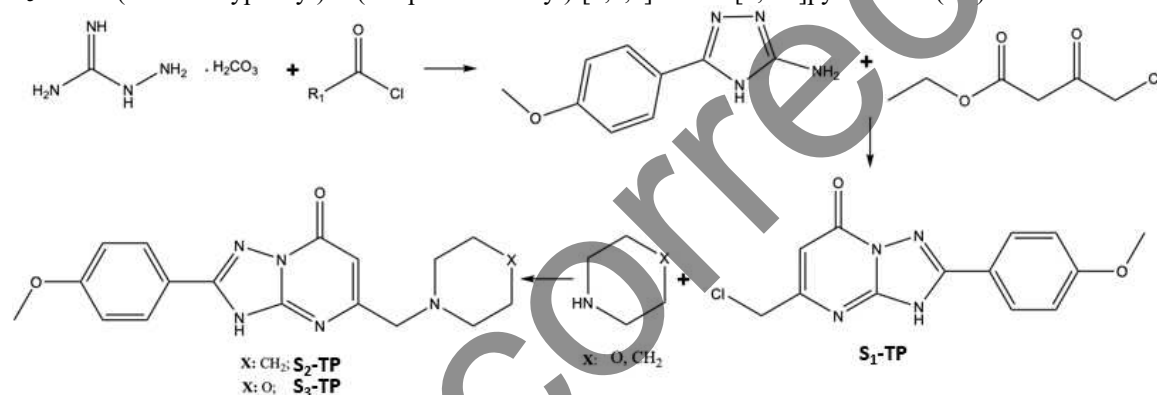


**Figure 1.** General synthesis scheme of the pyrimidinone-triazole derivatives: S<sub>1</sub>-TP, S<sub>2</sub>-TP, and S<sub>3</sub>-TP.

The characterization results are presented in supplementary information.

#### 2.3.2 Electrochemical Investigation of the Drug Candidates

+1.4 V potential for 30 s was applied to activate and clean the PGEs. 1000  $\mu\text{g/mL}$  of dsDNA was prepared with TE buffer and diluted with ACB. 1000  $\mu\text{g/mL}$  of drug candidates were prepared in dimethylformamide (DMF) and diluted to with proper buffers. These solutions were then added to the electrochemical measuring cell. Activated PGEs were dipped in these solutions, and DPV measurements were performed.

### 2.3.3 Interaction

Solutions containing 50  $\mu\text{g/mL}$  of dsDNA and 10  $\mu\text{g/mL}$  of drug candidates were mixed in ACB (pH: 3.8 for  $S_1$ -TP/DNA,  $S_2$ -TP/DNA; and pH: 5.6 for  $S_3$ -TP/DNA). The solutions were then placed in the thermal shaker at 600 rpm and 45°C for 30 min. Then, 100  $\mu\text{L}$  of this interaction solution was put into the tubes. The PGEs were dipped in the interaction solutions for 30 min. Then, DPV measurements were performed.

### 2.3.4 Measurement

DPV and CV measurements were performed from +0.4 and +1.4 V at 100 mV/s scan rate with 0.5 s interval time. The experimental steps are illustrated in Figure 2.

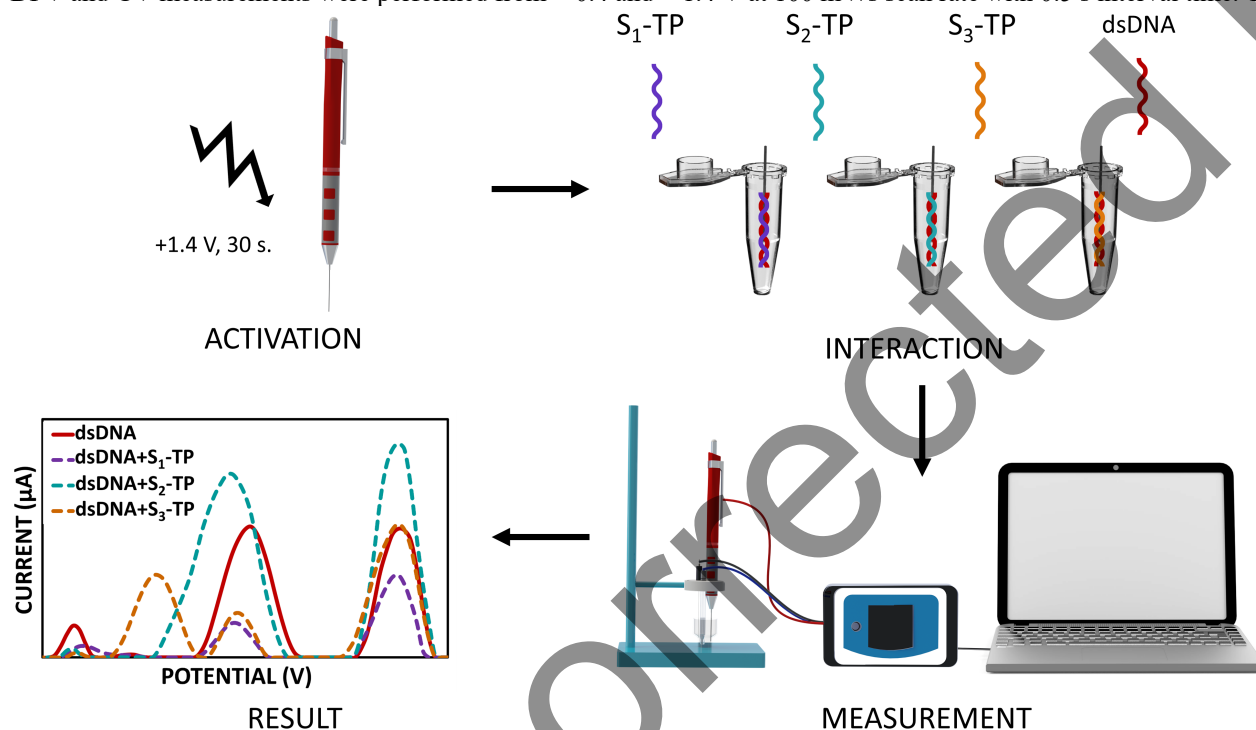


**Figure 2.** Experimental steps: Activation of PGE with ACB, Interaction of dsDNA with  $S_1$ -TP,  $S_2$ -TP and  $S_3$ -TP, and DPV measurements.

## 3. RESULTS AND DISCUSSION

### 3.1. Synthesis of Compounds

Three novel drug candidates were synthesized as below:

5-(Chloromethyl)-2-(4-methoxyphenyl)-[1,2,4]triazolo[1,5-*a*]pyrimidin-7(3*H*)-one ( $S_1$ -TP).

Yellow solid; yield, 52 %; m.p., 113 °C;  $^1\text{H-NMR}$  (DMSO- $d_6$ , 400 MHz)  $\delta$  8.02 (d,  $J = 8.7$  Hz, 2H), 7.07 (d,  $J = 8.8$  Hz, 2H), 6.16 (s, 1H), 4.66 (s, 2H), 3.81 (s, 3H) ppm;  $^{13}\text{C-NMR}$  (DMSO- $d_6$ , 100 MHz)  $\delta$  161.6, 156.1, 151.8, 128.7, 114.8, 100.4, 55.8 ppm; C<sub>13</sub>H<sub>11</sub>CIN<sub>4</sub>O<sub>2</sub> HRMS  $m/z$ : 290.0552 (Calcd for 290.05705)

#### **2-(4-Methoxyphenyl)-5-(piperidinomethyl)-[1,2,4]triazolo[1,5-*a*]pyrimidin-7(3*H*)-one (S<sub>2</sub>-TP)**

Yellow solid; yield, 30 %; m.p., 128 °C;  $^1\text{H-NMR}$  (DMSO- $d_6$ , 400 MHz)  $\delta$  8.01 (d,  $J = 8.7$  Hz, 2H), 6.99 (d,  $J = 8.8$  Hz, 2H), 5.63 (s, 1H), 3.79 (s, 3H), 3.30 (s, 2H), 3.23 (s, 2H), 2.34-2.42 (m, 2H), 1.50 (p,  $J = 5.5$  Hz, 4H), 1.34-1.43 (m, 2H) ppm;  $^{13}\text{C-NMR}$  (DMSO- $d_6$ , 100 MHz)  $\delta$  162.39, 160.28, 159.72, 158.74, 128.12, 125.96, 114.21, 94.35, 65.34, 55.59, 54.70, 26.19, 24.47 ppm; C<sub>18</sub>H<sub>21</sub>N<sub>5</sub>O<sub>2</sub> HRMS  $m/z$ : 339.16979 (Calcd for 339.16952).

#### **2-(4-Methoxyphenyl)-5-(morpholinomethyl)-[1,2,4]triazolo[1,5-*a*]pyrimidin-7(3*H*)-one (S<sub>3</sub>-TP)**

Yellow solid; yield, 35 %; m.p., 103 °C;  $^1\text{H-NMR}$  (DMSO- $d_6$ , 400 MHz)  $\delta$  8.02 (d,  $J = 8.9$  Hz, 2H), 6.99 (d,  $J = 8.9$  Hz, 2H), 5.66 (s, 1H), 3.79 (s, 3H), 3.53-3.65 (m, 4H), 3.28 (s, 2H), 2.37-2.47 (m, 4H) ppm;  $^{13}\text{C-NMR}$  (DMSO- $d_6$ , 100 MHz)  $\delta$  161.27, 160.51, 160.34, 159.55, 158.65, 128.16, 125.82, 114.23, 94.76, 66.76, 64.72, 55.59, 53.91 ppm; C<sub>17</sub>H<sub>19</sub>N<sub>5</sub>O<sub>3</sub> HRMS  $m/z$ : 341.14814 (Calcd for 341.14879).

The designed compounds were synthesized in three steps (Figure 1). The structures of the final compounds were determined by spectral analyses and the spectroscopic data confirmed the proposed structures. In the  $^1\text{H NMR}$  spectra, hydrogen atom of the heterocyclic ring was observed as a singlet signal between  $\delta$  5.63–6.16 ppm. The methylene protons, attached to heterocyclic ring at 5 positions, were observed as singlet with two proton integrals between  $\delta$  4.66 – 3.28 ppm. Proton signals of the benzene ring and cyclic amines were identified in the expected chemical shifts with expected divisions. The observed carbon signals in the  $^{13}\text{C NMR}$  of the compounds were in accordance with the target compounds. The amide carbon signal was observed between  $\delta$  161–162 ppm in  $^{13}\text{C NMR}$  spectrums.

The purity of the compounds was determined with HRMS spectra. The HRMS data were in accordance with the molecular formula and a found value within 0.003  $m/z$  unit of the calculated value of a parent-derived ion. S<sub>2</sub>-TP and S<sub>3</sub>-TP were introduced earlier in the literature (19), while the full spectral characterization of these compounds was for the first time introduced in this article.

### **3.2 Electrochemical Properties of Drug Candidates**

In this part, the electrochemical behaviors of the drug candidates were analyzed with DPV. As pH is quite important for the metabolism of drug molecules, the effect of pH on the oxidation signals of drug candidates was examined and the obtained results were shown in Figure 3.

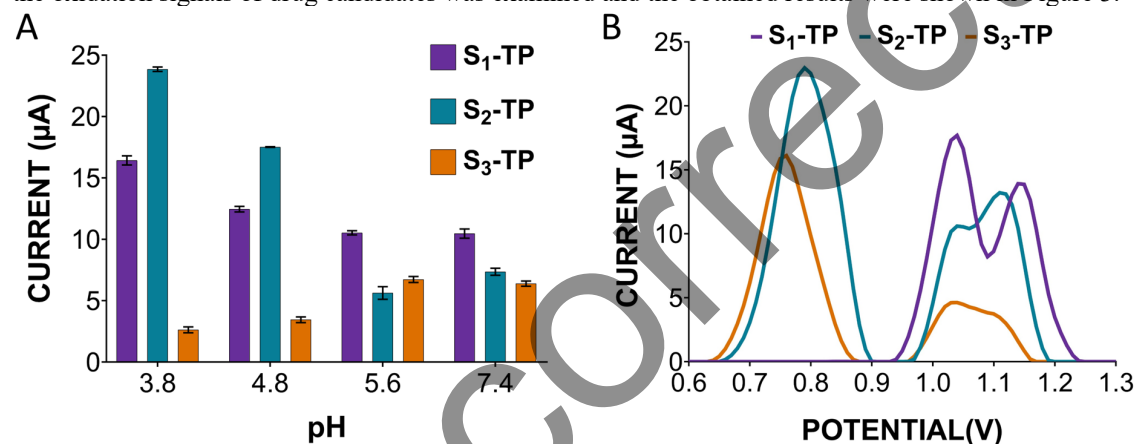


**Figure 3.** (A) Effect of pH on peak currents. Bar graphs: drug candidates in different pH values, 3.8 to 7.4. (B) DPV voltammogram of S<sub>1</sub>-TP, S<sub>2</sub>-TP, and S<sub>3</sub>-TP prepared in ACB (pH: 3.8 for S<sub>1</sub>-TP and S<sub>2</sub>-TP, and pH: 5.6 for S<sub>3</sub>-TP).

For the pH study in DPV, drug candidates were prepared using buffers with pH ranges from 3.8 to 7.4. As shown in Figure 3A, S<sub>1</sub>-TP and S<sub>2</sub>-TP produced stable responses, and the highest currents were obtained at pH 3.8. S<sub>3</sub>-TP showed the highest electrochemical signals at pH 5.6. Thus, pH 5.6 was chosen for the dilution buffer for S<sub>3</sub>-TP (Figure 3A).

At pH 3.8, the oxidation peak potentials of S<sub>1</sub>-TP were detected at 1.03 V and 1.15 V. As it is more stable and higher, the signal obtained at 1.03 V was chosen as the main oxidation signal for further studies. At pH 3.8, S<sub>2</sub>-TP gave two oxidation signals at 0.79 V and 1.11 V. At pH 5.6, the oxidation peak potentials of S<sub>3</sub>-TP were observed at 0.76 V and 1.04 V (Figure 3B). All oxidation signals were shifted to lower potentials with pH. These shifts in peak potentials for drugs demonstrate that protons participate in the oxidation process of drugs (20).

As shown in Figure 3B, all drug candidates have oxidation capacity. Triazolopyrimidinone structure could form triazolopyrimidinol by an H atom shifting, tautomerization. Several factors could contribute to the stability between two tautomers, e.g., substitution, aromaticity, hydrogen bonding, and solvation. The redox mechanism of these novel agents on graphite electrode surfaces could involve the oxidation of phenol groups of the compounds. Heteroatoms in the substituted amines might also contribute to the oxidation potency of the compounds, e.g., they could change the oxidation potency. Considering the phenolic tautomerization of the heteroaromatic ring and the amine substitution, the title compound could possess oxidative properties.

In the second part of our study, DPV measurements were performed at different concentrations of drug candidates at 100 mV/s to determine the analytical concentration ranges for the drug candidates (Figure 4).

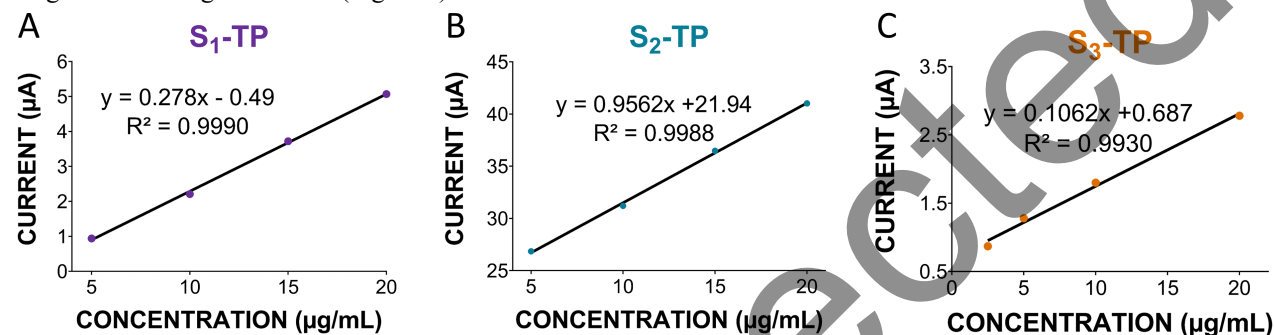


**Figure 4.** Calibration graphs for (A) S<sub>1</sub>-TP, (B) S<sub>2</sub>-TP, and (C) S<sub>3</sub>-TP obtained from drug concentration vs. current peak data.

The formulas for calculating Limit of detection (LOD) and limit of quantification (LOQ) depend on the specific method used, but generally, LOD is calculated as 3 times the standard deviation of the response (ss) divided by the slope of the calibration curve (m), while LOQ is calculated as 10 times the standard deviation of the response divided by the slope of the calibration curve'.

$$\text{LOD} = 3s/m$$

$$\text{LOQ} = 10s/m$$

LOD and LOQ were determined from Figure 4. For S<sub>1</sub>-TP and S<sub>2</sub>-TP, LOD and LOQ were calculated from the concentrations 5, 10, 15, and 20 µg/mL. For S<sub>3</sub>-TP, LOD and LOQ were calculated from the concentrations 2.5, 5, 10, and 20 µg/mL. LOD and LOQ for S<sub>1</sub>-TP are 1.5 µg/mL and 5.0 µg/mL, respectively (Figure 4A). LOD and LOQ for S<sub>2</sub>-TP are 1.0 µg/mL and 3.4 µg/mL, respectively (Figure 4 B). LOD and LOQ for S<sub>3</sub>-TP are 2.0 µg/mL and 6.8 µg/mL, respectively (Figure 4C). The correlation coefficients are 0.9990, 0.9988, and 0.9930 for S<sub>1</sub>-TP, S<sub>2</sub>-TP, and S<sub>3</sub>-TP, respectively.

The effects of scan rate (V) on peak current (I<sub>p</sub>) were studied using CV between 25-150 mV/s as shown in Figure 5.

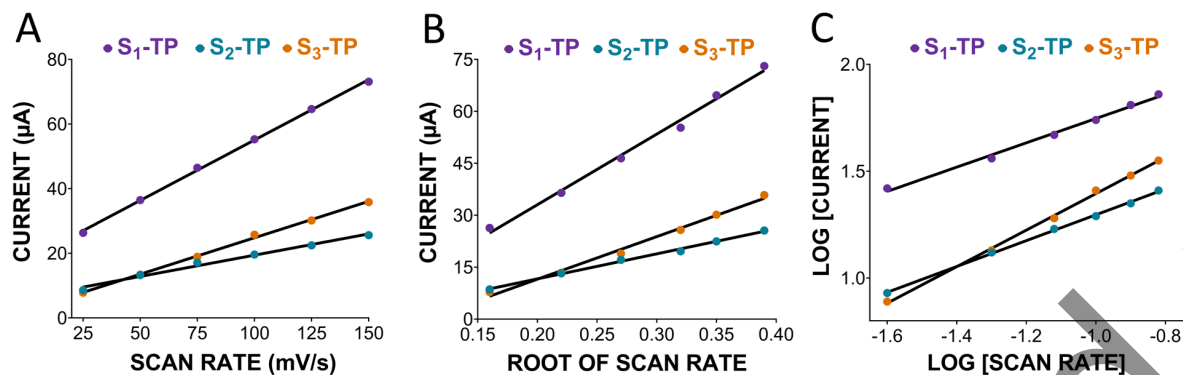


**Figure 5:** Effect of (A) scan rate and (B) scan rate root on peak current, and (C) scan rate on the log of peak current.

As shown in Figure 5A, the anodic peak current ( $I_{pa}$ ) has a linear relationship with scan rate ( $v$ ):

$$S_1\text{-TP: } I_{pa} (\mu\text{A}) = 0.374v + 17.666 \quad (R^2=0.9990) \quad (\text{Equation 1})$$

$$S_2\text{-TP: } I_{pa} (\mu\text{A}) = 0.1316v + 6.2628 \quad (R^2=0.9880) \quad (\text{Equation 2})$$

$$S_3\text{-TP: } I_{pa} (\mu\text{A}) = 0.2254v + 2.2687 \quad (R^2=0.9980) \quad (\text{Equation 3})$$

As shown in Figure 5B, peak current ( $I_{pa}$ ) also has a linear relationship with the root of the scan rate ( $v^{1/2}$ ):

$$S_1\text{-TP: } I_{pa} (\mu\text{A}) = 203.97v^{1/2} - 7.7443 \quad (R^2=0.9928) \quad (\text{Equation 4})$$

$$S_2\text{-TP: } I_{pa} (\mu\text{A}) = 72.771v^{1/2} - 2.9923 \quad (R^2=0.9977) \quad (\text{Equation 5})$$

$$S_3\text{-TP: } I_{pa} (\mu\text{A}) = 122.95v^{1/2} - 13.05 \quad (R^2=0.9920) \quad (\text{Equation 6})$$

In Figure 5C,  $\log(I_{pa})$  and  $\log(v)$  linear relationship was presented within the scan rate range between 25 mV/s and 150 mV/s:

$$S_1\text{-TP: } \log I_{pa} = 0.5716 \log v + 2.3213 \quad (R^2=0.9937) \quad (\text{Equation 7})$$

$$S_2\text{-TP: } \log I_{pa} = 0.5996 \log v + 1.899 \quad (R^2=0.9987) \quad (\text{Equation 8})$$

$$S_3\text{-TP: } \log I_{pa} = 0.8568 \log v + 2.2551 \quad (R^2=0.9978) \quad (\text{Equation 9})$$

According to the literature, these slope values are close to the theoretical value, e.g., 0.5, indicating the diffusion-controlled processes, while for the theoretical value 1, the process is adsorption-controlled (21). Slopes of Equation 7 and Equation 8 were determined as 0.5716 and 0.5996, respectively, which indicates that electrochemical oxidations of  $S_1\text{-TP}$  and  $S_2\text{-TP}$  are diffusion-controlled processes. According to Equation 9, the slope is 0.8568, which proves that the electrode process was adsorption controlled for  $S_3\text{-TP}$ .

### 3.3 INTERACTION

The intrinsic electro-activity of adenine and guanine bases are generally used as an indicator for drug-DNA interactions. In the next step of our study, we studied the interaction of drug candidates with dsDNA. 100  $\mu\text{g/mL}$  dsDNA solutions were prepared with TE buffer (pH: 8.0).

The stock drug solutions were prepared with DMF and diluted with ACB (pH: 3.8 for  $S_1\text{-TP}$  and  $S_2\text{-TP}$ , and pH: 5.6 for  $S_3\text{-TP}$ ). The final concentrations of dsDNA and  $S\text{-TP}$  were 50  $\mu\text{g/mL}$  and 10  $\mu\text{g/mL}$ , respectively. All solutions were placed in the thermal shaker, where stirring was applied at 600 rpm and 45  $^\circ\text{C}$  for 30 min. Then, 100  $\mu\text{L}$  of the solution was transferred into tubes, and the electrodes were immersed in these tubes for 30 min. Oxidation signals were measured with DPV in the range between 0 and 1.4 V at 50 mV/s scan rate in the absence and the presence of drug candidate molecules. The analytical signals associated with the guanine bases of DNA were obtained at  $\sim 1.0$  V vs. Ag/AgCl.

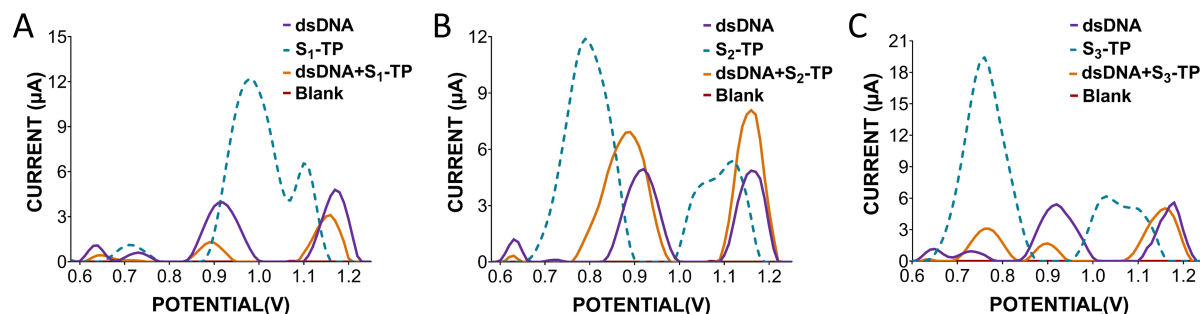


**Figure 6.** Differential pulse voltammograms of guanine oxidation currents of dsDNA after interaction with (A) S<sub>1</sub>-TP, (B) S<sub>2</sub>-TP, and (C) S<sub>3</sub>-TP. Experimental steps are: PGE pretreatment: 1.4 V for 30 s, Interaction: 100 µg/mL of dsDNA and 20 µg/mL of drug candidates, Stirring: 600 rpm at 45 °C for 30 min, Adsorption: 30 min, and DPV measurement within a range between 0 and +1.4 V at 50 mV/s in ACB.

In Figure 6A, two distinct oxidation signals associated with dsDNA in ACB (pH: 3.8) were obtained at +0.92 V and +1.17 V, respectively. After the interaction with S<sub>1</sub>-TP, the peak potential of dsDNA shifted to +0.89 V and +1.16 V, respectively. On the other hand, after the interaction with S<sub>2</sub>-TP, one of the peak potentials of dsDNA shifted negatively from +0.92 V to +0.89 V. Oxidation signals of dsDNA in ACB (pH: 5.6) were obtained at +0.92 V and +1.18 V. In the presence of S<sub>3</sub>-TP, the peak potentials of dsDNA slightly shifted toward smaller values, e.g., +0.90 V and +1.16 V (Figure 6C). dsDNA oxidation potentials shifted negatively after interacting with S<sub>1</sub>-TP, S<sub>2</sub>-TP and S<sub>3</sub>-TP. Here, positive or negative shifts on peak potential can reveal the interaction mechanism between the drug candidate and dsDNA. Positive peak potential shifts are associated with intercalative binding, while negative peak potential shifts are associated with electrostatic binding (22). Bilge et al. reported the interaction mechanism between ibrutinib (IBR) and dsDNA using electrochemical and molecular docking techniques. Voltametric studies indicated that the peak potential of IBR shifting towards less positive potentials as a result of electrostatic interaction (23). In our study, the shift in the peak potential towards the negative could be attributed to the irreversible electrode process (24). The reason for this shift could be explained by electrostatic binding between S<sub>s</sub>-TP and dsDNA.

In Figure 6A, the peak currents of dsDNA were found as 3.95 µA and 4.79 µA with the relative standard deviation (RSD) 5.45%, 3.76% which decreased to 1.30 µA and 3.11 µA after the interaction with RSD 3.12%, 4.87% (n=5). In Figure 6B, the peak currents of dsDNA were found as 4.94 µA and 4.86 µA with RSD 1.68%, 4.54% which increased, e.g., 6.92 µA with RSD 3.95%, 7.62% and 8.08 µA with RSD 1.49%, 5.23%, due to the binding of S<sub>2</sub>-TP to dsDNA, changing the dsDNA structure. Figure 6C demonstrates that S<sub>3</sub>-TP caused a significant change in the oxidation currents of dsDNA. Here, the peak currents of dsDNA are as 5.42 µA with RSD 2.97%, and 5.58 µA with RSD 7.66% while after interaction we determined three peaks at 3.07 µA with RSD 5.22%, 1.66 µA with RSD 9.13%, and 5.03 µA with RSD 4.68%

### 3.4 STABILITY

Stability is one of the most important factors that are related to the efficacy of drug candidates. To evaluate the stability of the drug candidates, we performed DPV (Figure 7). The stock solutions of drug candidates were freshly prepared and stored in dark at room temperature (25 °C). Stock solutions of drug candidates measured within 0, 5, 7, 14, and 30 days. Here, S<sub>1</sub>-TP and S<sub>3</sub>-TP exhibited good stability for 30 days of storage without significant percentage changes in current values, e.g., we observed a slight reduction in the percentage of current for S<sub>1</sub>-TP between day 0 and 30. At the end of day 30, the percentage of the current value for S<sub>1</sub>-TP was determined as 91%. A noticeable change in the percentage current of S<sub>2</sub>-TP was observed at day 30, e.g., 48%. In contrast, minute changes in current values of S<sub>2</sub>-TP were observed between day 7 and 30, e.g., the current value of S<sub>3</sub>-TP decreased to 86% at day 30. These results proved that the stock solutions of drugs were stable for 30 days, except S<sub>2</sub>-TP, which could be very advantageous for long-term use by retaining their pharmaceutical properties.

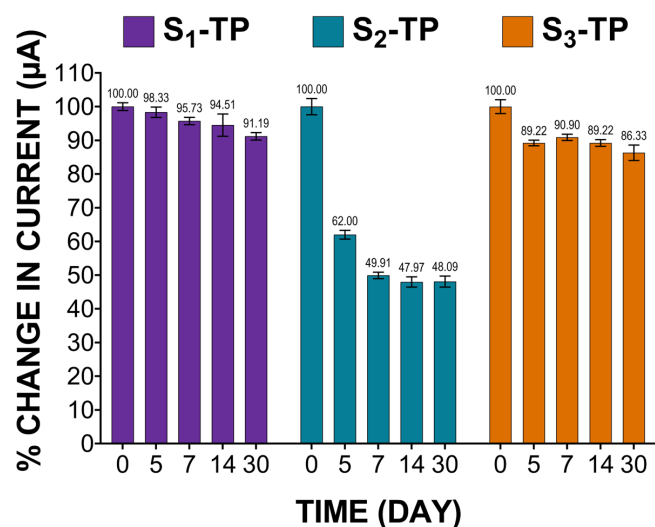


**Figure 7.** Change in current for S<sub>1</sub>-TP, S<sub>2</sub>-TP, and S<sub>3</sub>-TP examined at 25 °C for different days, e.g., 0, 5, 7, 14, and 30. Percentage current values of drug candidates were 91%, 48%, and 86% by the end of 30 days, respectively.

#### 4. CONCLUSION

In conclusion, in this article, we for the first time studied the full characterization of S<sub>1</sub>-TP, S<sub>2</sub>-TP and S<sub>3</sub>-TP compounds. Importantly, S<sub>1</sub>-TP is reported for the first time in the literature, while S<sub>2</sub>-TP and S<sub>3</sub>-TP compounds were reported in the literature for only their screening activity against FABPs (Patent No; WO 2010/056630 A1). We introduced the synthetic pathway and full spectral characterization data of these compounds to the literature. Our article focused on the electrochemical behaviors of S<sub>s</sub>-TP and their interactions with dsDNA using DPV and CV. We showed the interaction of S<sub>s</sub>-TP–dsDNA resulted in significant changes on dsDNA peak potential. dsDNA peak potential shifted negatively after the interaction with S<sub>1</sub>-TP, S<sub>2</sub>-TP, and S<sub>3</sub>-TP. The shift of dsDNA peak potential reveals the interaction of S<sub>s</sub>-TP with DNA supporting the binding in between. Moreover, the shift in the peak potential of dsDNA towards more positive values indicates that DNA-drug interaction mechanism is intercalation, while the shift towards more negative value indicates that DNA-drug interaction mechanism is an electrostatic mode. Our study also showed that electrochemical oxidation processes of S<sub>1</sub>-TP and S<sub>2</sub>-TP were irreversible and controlled by diffusion. In addition, the electron transfer process was an adsorption-controlled process for S<sub>3</sub>-TP. We believe our study can provide critical information for understanding the DNA-drug interaction that could be very advantageous to analyze new drug compounds and their potential effect on target biomolecules.

#### REFERENCES

1. Aggarwal R, Sumran G. An insight on medicinal attributes of 1,2,4-triazoles. *Eur J Med Chem.* 2020;205:112652.
2. Janganati V, Ponder J, Balasubramaniam M, Bhat-Nakshatri P, Bar EE, Nakshatri H, et al. MMB triazole analogs are potent NF-κB inhibitors and anti-cancer agents against both hematological and solid tumor cells. *Eur J Med Chem.* 2018;157:562–81.
3. Huo JL, Wang S, Yuan XH, Yu B, Zhao W, Liu HM. Discovery of [1,2,4]triazolo[1,5-a]pyrimidines derivatives as potential anticancer agents. *Eur J Med Chem.* 2021;211:113108.
4. Fandzloch M, Jędrzejewski T, Dobrzańska L, Esteban-Parra GM, Wiśniewska J, Paneth A, et al. New organometallic ruthenium(ii) complexes with purine analogs - a wide perspective on their biological application. *Dalt Trans.* 2021;50(16):5557–73.
5. Ruta LL, Farcasanu IC, Bacalum M, Răileanu M, Rostas AM, Daniliuc C, et al. Biological activity of triazolopyrimidine copper(I) complexes modulated by an

auxiliary n-n-chelating heterocycle ligands. *Molecules*. 2021;26(22).

6. Harrison D, Bock MG, Doedens JR, Gabel CA, Holloway MK, Lewis A, et al. Discovery and Optimization of Triazolopyrimidinone Derivatives as Selective NLRP3 Inflammasome Inhibitors. *ACS Med Chem Lett*. 2022;13(8):1321–8.
7. Beniaminov AD, Chashchina G V., Livshits MA, Kechko OI, Mitkevich VA, Mamaeva OK, et al. Discrimination between g/c binding sites by olivomycin a is determined by kinetics of the drug-DNA interaction. *Int J Mol Sci*. 2020;21(15):1–14.
8. Erol A, Akpınar F, Muti M. Electrochemical determination of anticancer drug Bendamustine and its interaction with double strand DNA in the absence and presence of quercetin. *Colloids Surfaces B Biointerfaces*. 2021;205:111884.
9. Ijäs H, Shen B, Heuer-Jungemann A, Keller A, Kostianen MA, Liedl T, et al. Unraveling the interaction between doxorubicin and DNA origami nanostructures for customizable chemotherapeutic drug release. *Nucleic Acids Res*. 2021;49(6):3048–62.
10. Kozieł SA, Lesiów MK, Wojtala D, Dyguda-Kazimierowicz E, Bieńko D, Komarnicka UK. Interaction between dna, albumin and apo-transferrin and iridium(III) complexes with phosphines derived from fluoroquinolones as a potent anticancer drug. *Pharmaceuticals*. 2021;14(7).
11. Morawska K, Popławski T, Ciesielski W, Smarżewska S. Electrochemical and spectroscopic studies of the interaction of antiviral drug Tenofovir with single and double stranded DNA. *Bioelectrochemistry*. 2018;123:227–32.
12. Nimal R, Nur Unal D, Erkmen C, Bozal-Palabiyik B, Siddiq M, Eren G, et al. Development of the electrochemical, spectroscopic and molecular docking approaches toward the investigation of interaction between DNA and anti-leukemic drug azacytidine. *Bioelectrochemistry*. 2022;146:108135.
13. Ponkarpagam S, Vennila KN, Elango KP. Molecular spectroscopic and molecular simulation studies on the interaction of oral contraceptive drug Ormeloxifene with CT-DNA. *Spectrochim Acta - Part A Mol Biomol Spectrosc*. 2022;278:121351.
14. Shahabadi N, Abbasi AR, Moshtkob A, Hadidi S. Design, synthesis and DNA interaction studies of new fluorescent platinum complex containing anti-HIV drug didanosine. *J Biomol Struct Dyn*. 2020;38(10):2837–48.
15. Wang W, Zhang Y, Liu D, Zhang HJ, Wang XF, Zhou Y. Prediction of DNA-Binding Protein-Drug-Binding Sites Using Residue Interaction Networks and Sequence Feature. *Front Bioeng Biotechnol*. 2022;10:1–10.
16. Agarwal S, Jangir DK, Mehrotra R. Spectroscopic studies of the effects of anticancer drug mitoxantrone interaction with calf-thymus DNA. *J Photochem Photobiol B Biol*. 2013;120:177–82.
17. Diculescu VC, Chiorcea-Paquim AM, Oliveira-Brett AM. Applications of a DNA-electrochemical biosensor. *TrAC - Trends Anal Chem*. 2016;79:23–36.
18. Istanbul H, Bayraktar G, Ozturk I, Coban G, Saylam M. Design, synthesis and bioactivity studies of novel triazolopyrimidinone compounds. *J Res Pharm*. 2022;26(1):231–42.
19. Nieman K, Us IL, Kenny H, Us IL. *Methods for Treating Ovarian Cancer by Inhibiting Fatty Acid Binding Proteins*. Vol. 2. 2014.
20. Deng P, Xu Z, Kuang Y. Electrochemically reduced graphene oxide modified acetylene black paste electrode for the sensitive determination of bisphenol A. *J Electroanal Chem*. 2013;707:7–14.
21. Jakóbczyk P, Dettlaff A, Skowierzak G, Ossowski T, Ryl J, Bogdanowicz R. Enhanced stability of electrochemical performance of few-layer black phosphorus electrodes by noncovalent adsorption of 1,4-diamine-9,10-anthraquinone. *Electrochim Acta*. 2022;416.
22. Sirajuddin M, Ali S, Badshah A. Drug-DNA interactions and their study by UV-Visible, fluorescence spectroscopies and cyclic voltametry. *J Photochem Photobiol B Biol*. 2013;124:1–19.
23. Bilge S, Dogan-Topal B, Taskin Tok T, Atici EB, Smağ A, Ozkan SA. Investigation of the interaction between anticancer drug ibrutinib and double-stranded DNA by electrochemical and molecular docking techniques. *Microchem J*. 2022;180.
24. Radi A, El Ries MA, Kandil S. Electrochemical study of the interaction of levofloxacin with DNA. *Anal Chim Acta*. 2003;495(1–2):61–7.

SUPPLEMENTARY INFORMATION

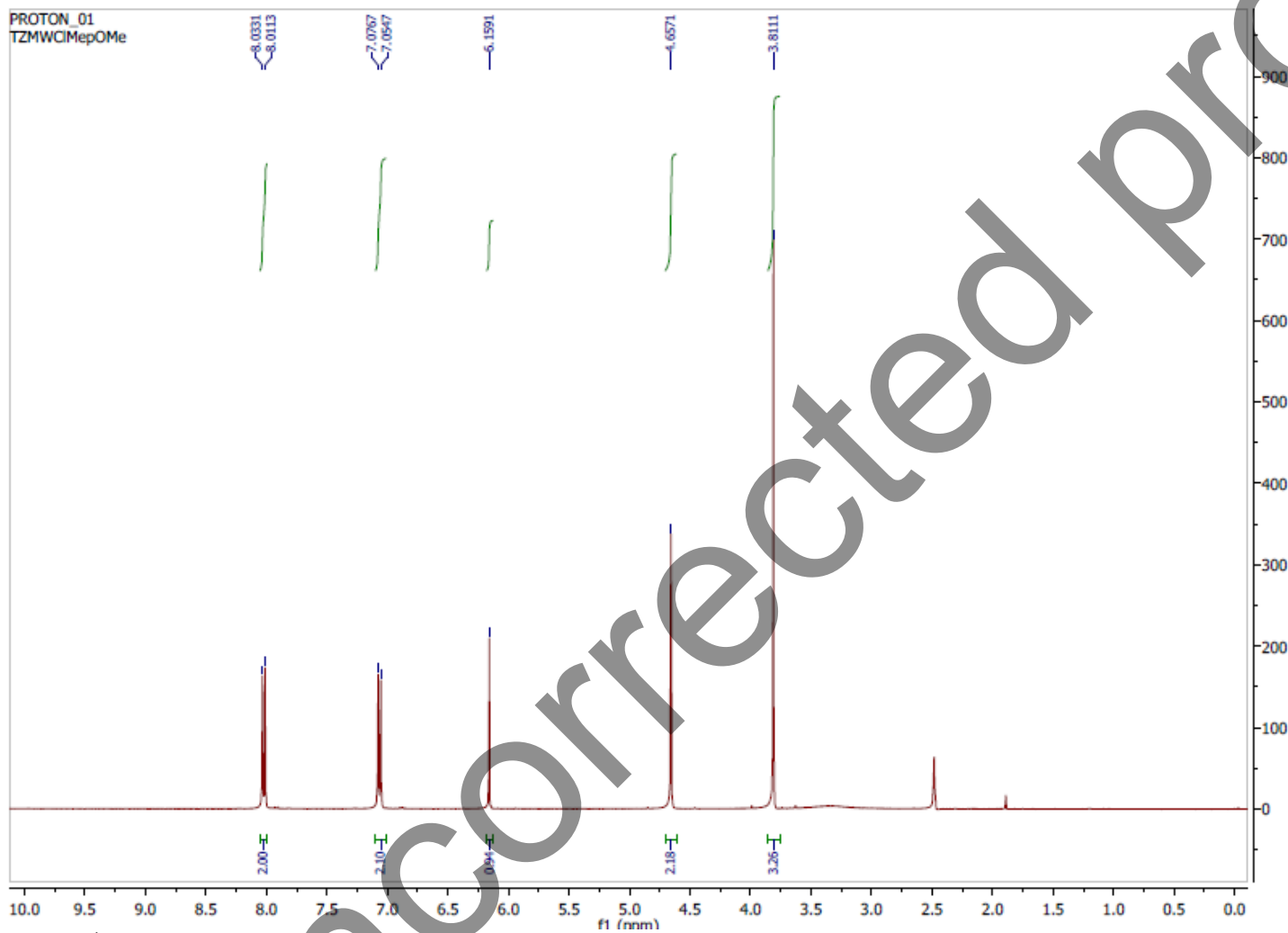


Figure 1. <sup>1</sup>H NMR Spectra of Si-TP.

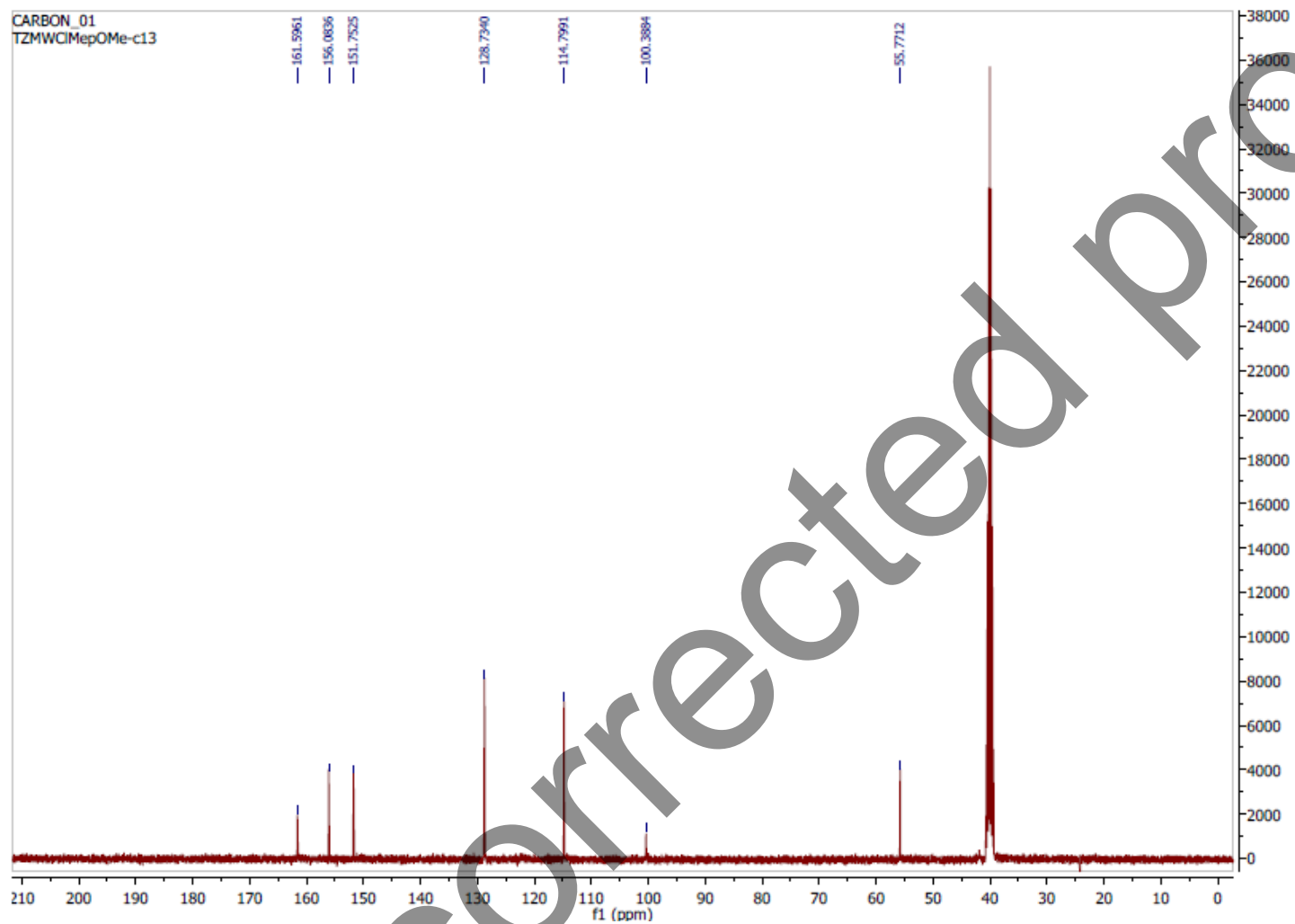
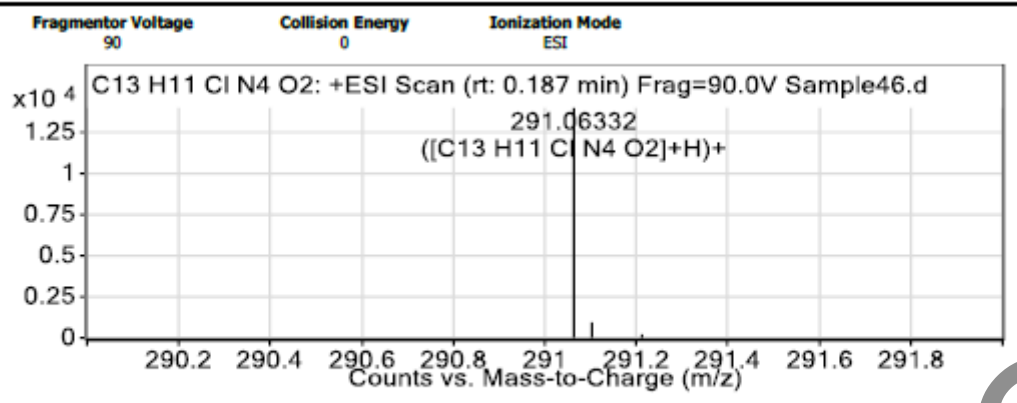


Figure 2. <sup>13</sup>C NMR Spectra of S1-TP.

User Spectra



Peak List

m/z	z	Abund	Formula	Ion
291.06332	1	13984.74	C13 H11 Cl N4 O2	(M+H)+
313.04364	1	22951.55		
315.04157	1	6561.68		
329.01804	1	7036.92		
603.10071	1	101639.05		
604.10314	1	28659.66		
605.09877	1	67451.13		
606.09997	1	16867.94		
607.09646	1	11783.25		
619.07417	1	9988.45		

Formula Calculator Element Limits

Element	Min	Max
C	3	13
H	0	11
N	0	4
O	0	2
Cl	0	1

Formula Calculator Results

Formula	Best	Mass	Igt Mass	Diff (ppm)	Ion Species	Score
C13 H11 Cl N4 O2	DOGRU	290.05552	290.05705	5.29	C13 H12 Cl N4 O2	80.21

Data Sheet. HRMS data of S1-TP

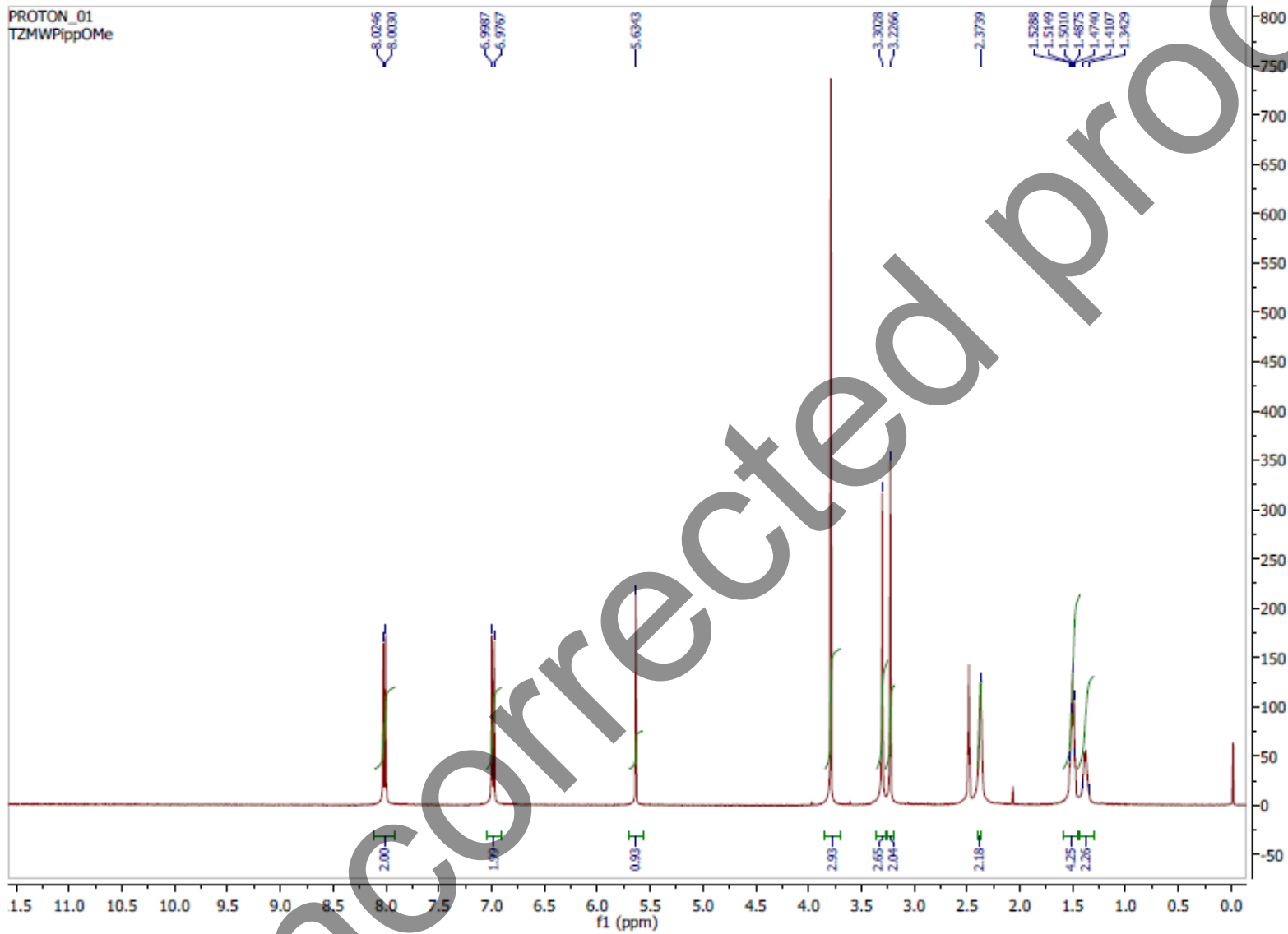


Figure 3. <sup>1</sup>H NMR Spectra of S<sub>2</sub>-TP

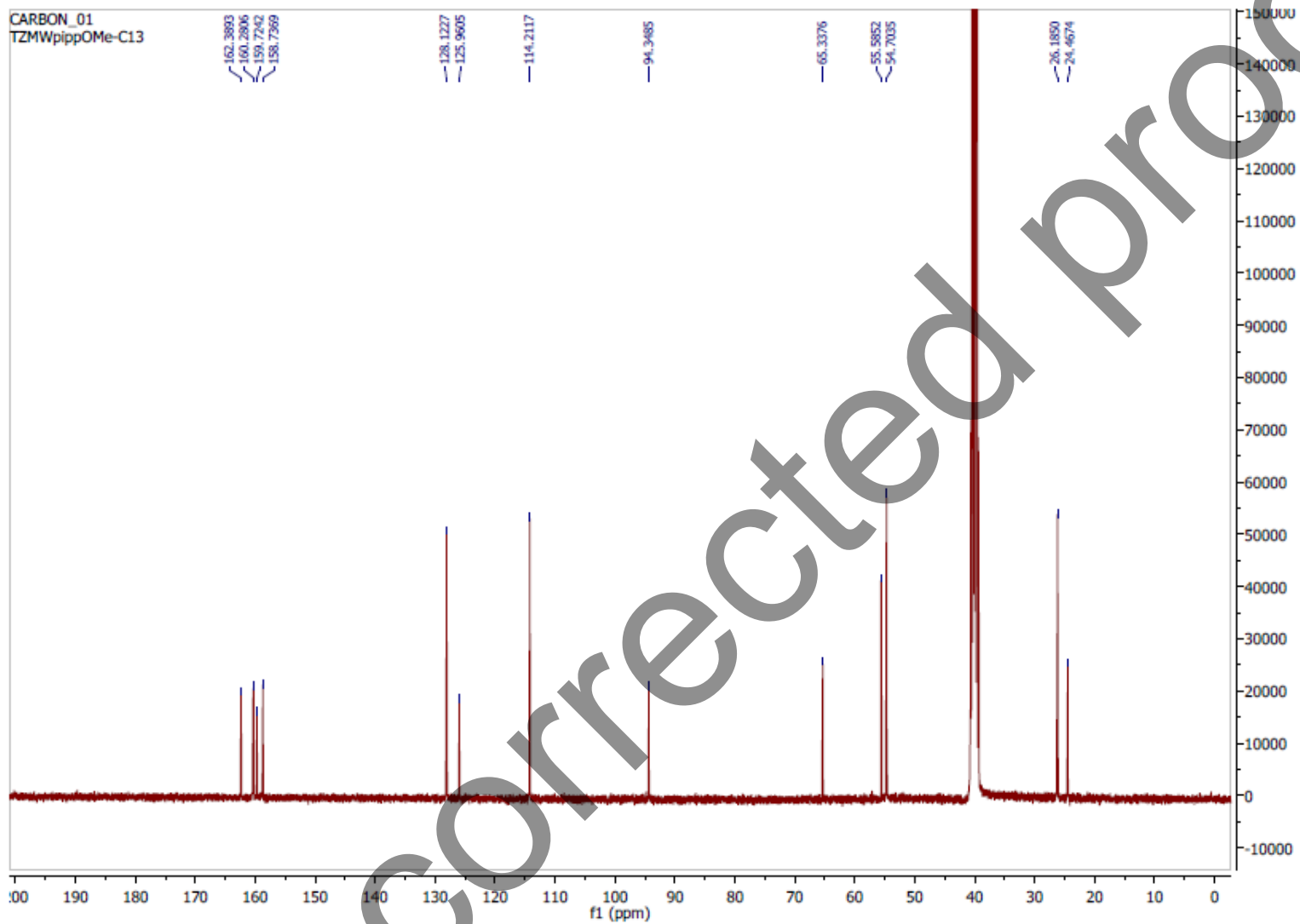
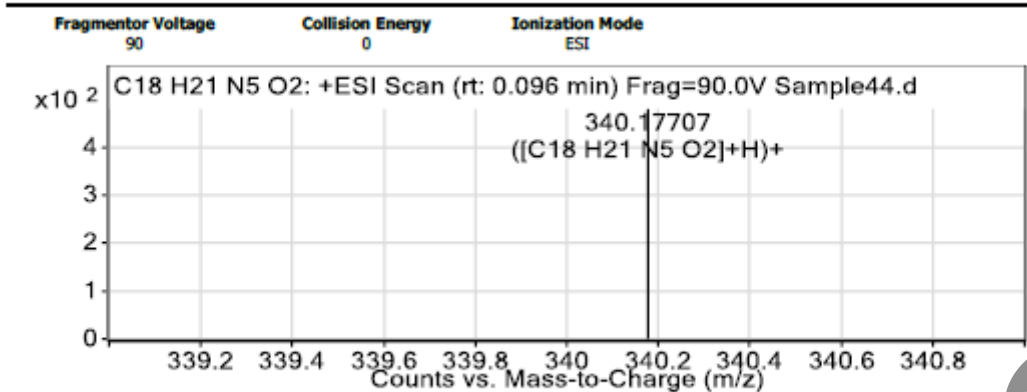


Figure 4. <sup>13</sup>C NMR Spectra of S<sub>2</sub>-TP

### User Spectra



#### Peak List

m/z	z	Abund
100.01216		716
101.00172		758.46
102.12696		2935.24
125.98556		819.45
130.15831		1208.29
167.01174		868.47
185.11372	1	2942.39
362.15579	1	2343.85
378.1331		684.14
406.32531	1	1478.49

#### Formula Calculator Element Limits

Element	Min	Max
C	3	18
H	0	21
N	0	5
O	0	2

#### Formula Calculator Results

Formula	Best	Mass	Tgt Mass	Diff (ppm)	Ion Species	Score
C18 H21 N5 O2	DOGRU	339.16979	339.16952	-0.8	C18 H22 N5 O2	47.39

Data Sheet. HRMS data of S<sub>2</sub>-TP

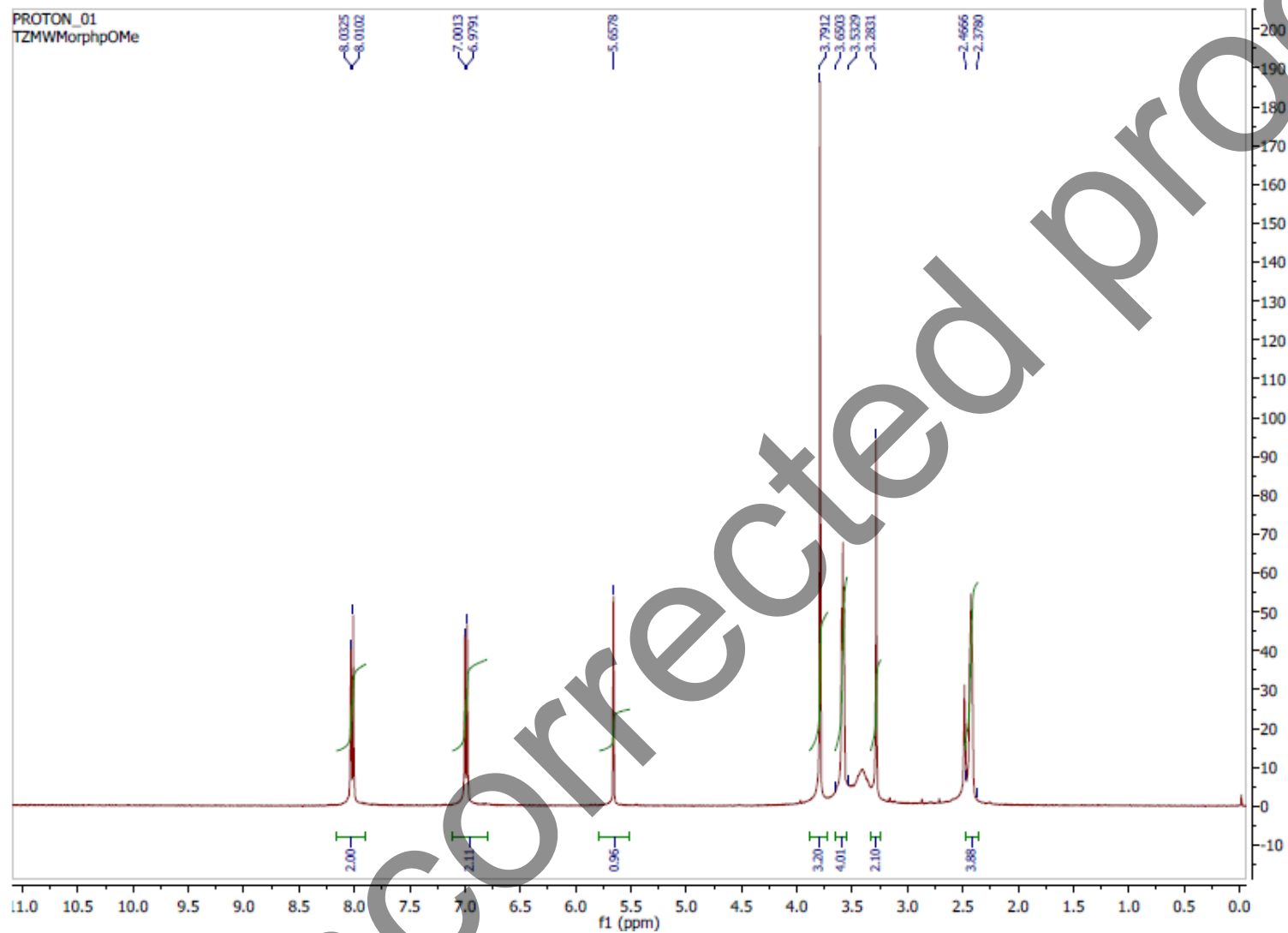


Figure 5. <sup>1</sup>H NMR Spectra of S<sub>3</sub>-TP

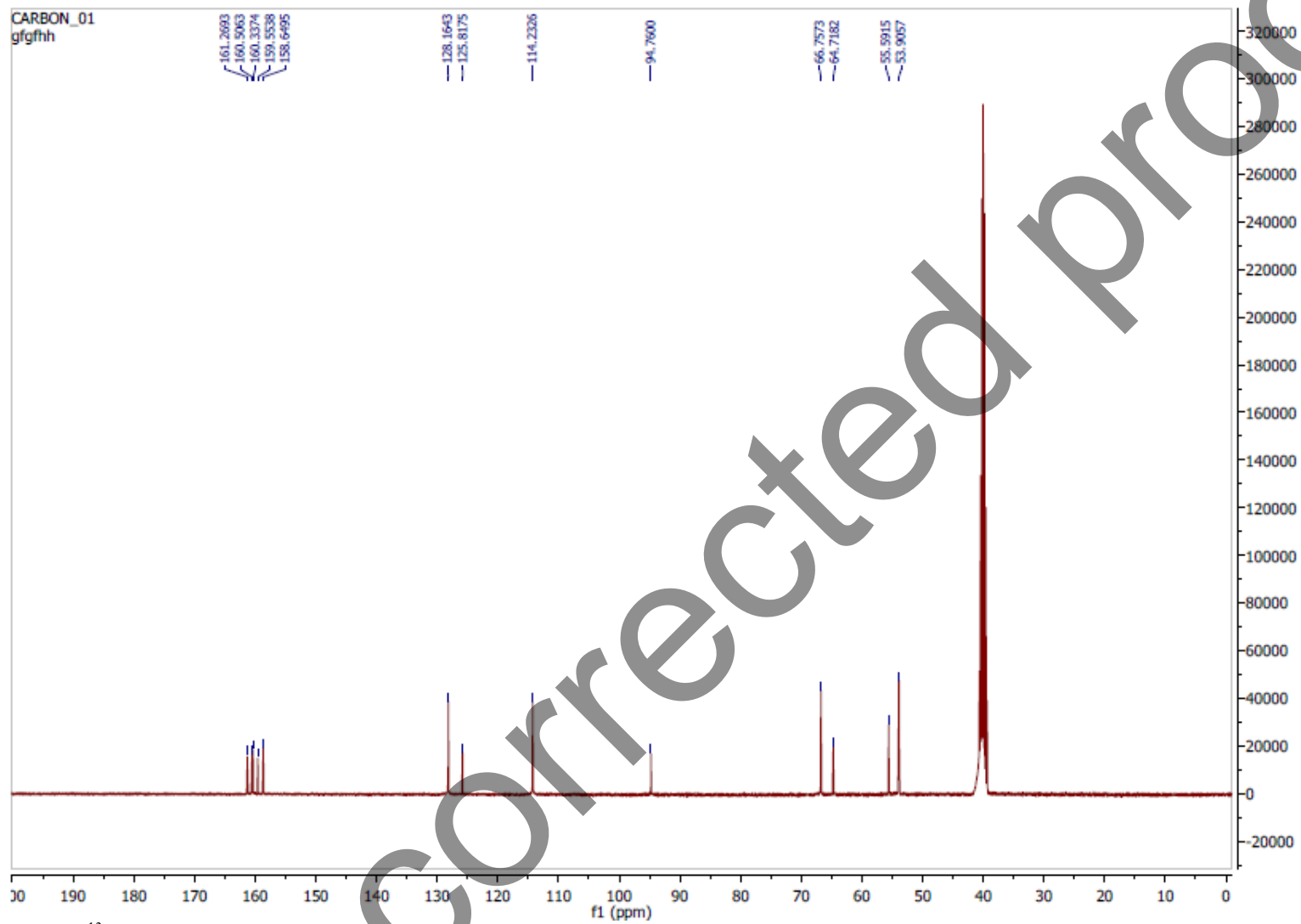
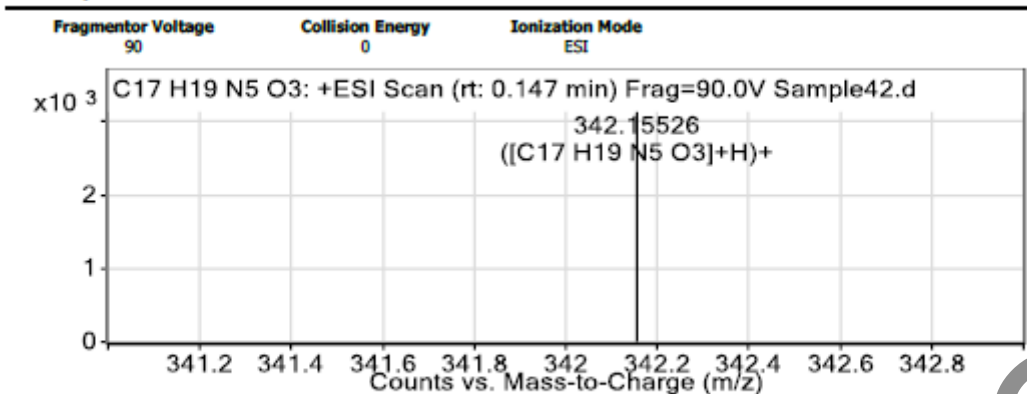


Figure 6. <sup>13</sup>C NMR Spectra of S<sub>3</sub>-TP

User Spectra



Peak List

m/z	z	Abund	Formula	Ion
132.90359		4762.14		
210.91546		1435.13		
342.15526	1	3130.95	C17 H19 N5 O3	(M+H)+
474.05149	1	16621.97		
474.10335		1299.25		
475.05505	1	2978.97		
547.10823	1	1285		
605.94806	1	4872.07		
683.30168	1	1764.2		
815.19928	1	3132.83		

Formula Calculator Element Limits

Element	Min	Max
C	3	17
H	0	19
N	0	5
O	0	3

Formula Calculator Results

Formula	Best	Mass	Igt Mass	Diff (ppm)	Ion Species	Score
C17 H19 N5 O3	DOGRU	341.14814	341.14879	1.89	C17 H20 N5 O3	83.48

Data Sheet. HRMS data of S<sub>3</sub>-TP